Synthesis, crystal structures, DFT studies, antibacterial assays and interaction assessments with biomolecules of new platinum(II) complexes with adamantane derivatives

Anna Karla dos Santos Pereira[a*], Carlos Marrote Manzano[a], Douglas Hideki Nakahata[a] Juan Carlos Tenorio Clavijo[a], Douglas Henrique Pereira[b], Wilton Rogério Lustri[c] and Pedro Paulo Corbi[a*].

[a] Institute of Chemistry, University of Campinas – UNICAMP, PO Box 6154, 13083-970 Campinas, SP, Brazil.

[b] Chemistry Collegiate, Federal University of Tocantins, Campus Gurupi, PO Box 66, Gurupi 77 402-970, Brazil.

[c] Department of Biological and Health Sciences, University of Araraquara, UNIARA, 14801-320, São Paulo, Brazil.

*Corresponding authors

E-mail:ppcorbi@unicamp.br / a209764@dac.unicamp.br

Contents

Infrared spectra

The infrared spectra of the complexes Pt-atd, Pt-rtd and Pt-mtn and their precursors are shown in Figure S1. The bands in the region of 2903-2841 cm^{-1} can be attributed to the ν(CH) and ν(CH_2) stretches of the adamantane cage[1] of the ligands. Bands in the region 3273-3104 cm^{-1} in the spectra of the complexes correspond to the asymmetric and symmetric (NH_2) stretching modes of the coordinated amino group[2]. These same bands are not evident in the spectra of the ligands because in this case they are in the hydrochloride form and, therefore, the stretching modes of the amino group ν(NH_3^+) are overlapped. The bands in the region between 1582-1565 cm^{-1} were attributed to δ(H-N-H) vibrations[3]. Strong bands of absorption in the region 1131-1110 cm^{-1} and 1034-1017 cm^{-1} were attributed to the νS=O and νC-S vibrations, respectively, which confirms sulfur coordination of DMSO molecule to the Pt(II) center[4]. Finally, the bands in the region 445-438 cm^{-1} can be attributed to the νPt-S vibration mode characteristic of platinum complexes with S-coordinated sulfoxides.[5]

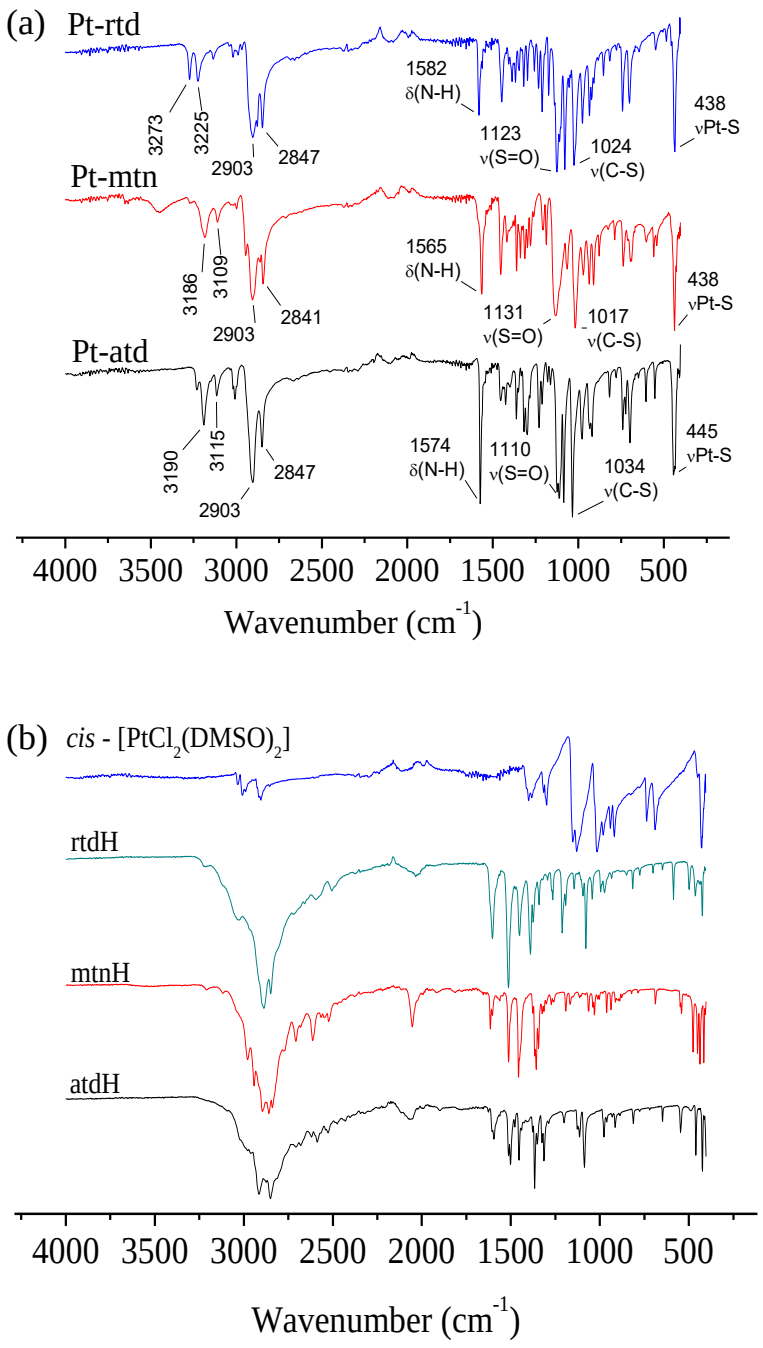

Figure S1. Infrared spectra of the (a) platinum(II) complexes and (b) precursors.

Thermogravimetric analysis

The thermogravimetric curves for the platinum complexes are shown in Figure S2. According to the experimental data, the Pt-atd compound starts to decompose at 160 °C with mass loss of 56.4% until 400 °C. The mass loss can be attributed to organic fraction of the molecule (calcd. 57.4%). The final residue corresponding to 42.6% is consistent with the formation of platinum oxide, PtO (calcd. 43.6%). For Pt-rtd compound, the thermal decomposition starts at 160 ºC with a mass loss of 44.10% from 160 - 257 °C, which is equivalent to the loss of rtd and DMSO molecules (calcd. 46.5%). There is a subsequent weight loss of 14.1% from 257 - 360 °C, which is consistent with the loss of two Cl atoms (calcd. 13.6%) with the formation of a final residue of 41.4%, which is consistent with platinum oxide, PtO (calcd. 40.3%). For Pt-mtn, there is a first step of mass loss of 2% from 25 to 120 °C, which was attributed to the loss of water or residual solvent. From 120 °C to 696 °C a mass loss of 54.8% was observed, which corresponds to the loss of one mtn and DMSO molecule and two Cl atoms (calcd. 59.7%). In 696 °C there is a residue of 41.4% which is consistent with the formation of PtO (calcd. 40.3%). From 696 °C to 900 °C there is a mass loss which, probably, corresponds to the reduction of PtO to Pt°. The thermal decomposition data are summarized in Table S1. The experimental thermogravimetric data reinforces the composition of the complexes as verified by elemental analyses and crystallographic data.

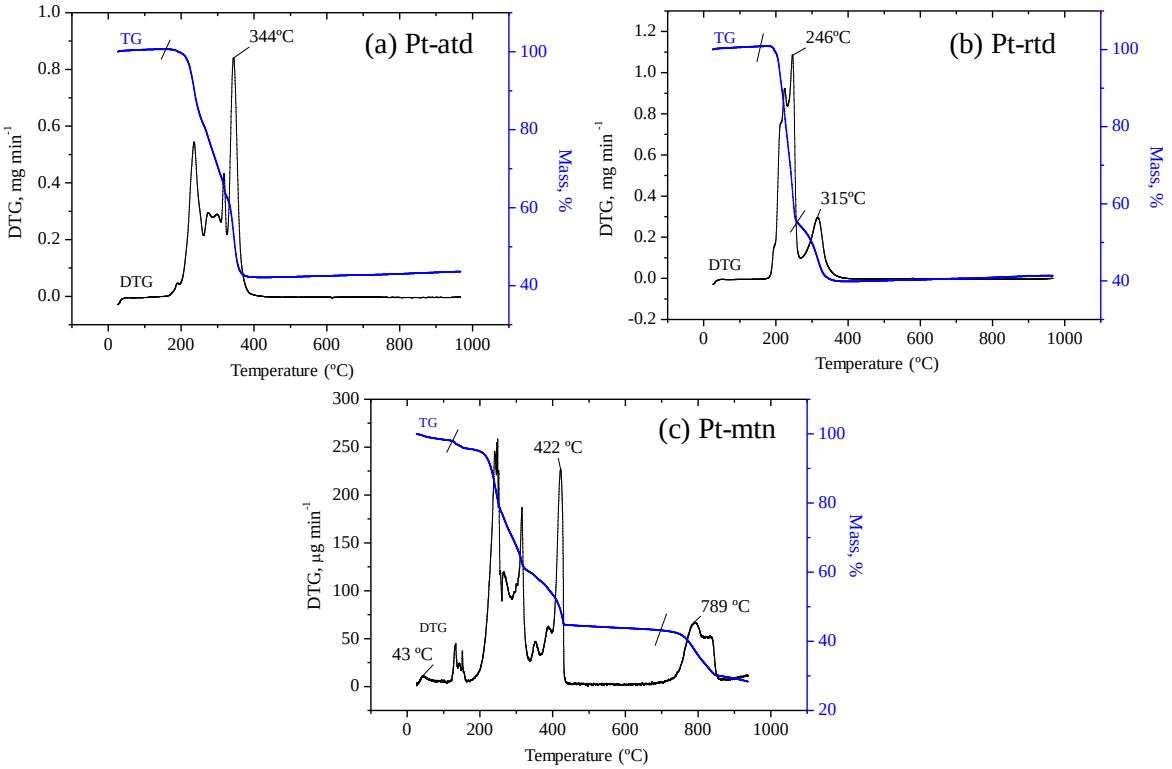

Figure S2. The TGA and DTG curves of (a) Pt-atd, (b) Pt-rtd and (c) Pt-mtn.

Table S1: Thermal behavior data of the complexes.

Complex	steps	Temperature range (ºC)	DTG peak	TG weight loss, %		Assignment
				Calcd.	Found	
Pt-atd	1st	160 – 400	344 ºC	57.4	56.4	Ligand + $(CH_3)_2SO$ + 2Cl
Residue				42.6	43.6	PtO
Pt-rtd	1st	160 – 257	246 ºC	46.1	44.5	Ligand +
	2nd	257 – 360	315 ºC	13.6	14.1	$(CH_3)_2SO$ + 2Cl
Residue				40.3	41.4	PtO
Pt-mtn	1st	26 – 120	43 ºC		2.00	Residual solvent
	2nd	120 – 696	422 ºC	59.7	54.8	Ligand + $(CH_3)_2SO$ + 2Cl
Residue				40.3	43.2	PtO
	3rd	696 – 900	789 ºC			Pt°

Crystallography

Table S2: Experimental details for crystal structure determination and refinement of Pt-atd, Pt-rtd and Pt-mtn.

Parameter	**Pt-atd**	**Pt-rtd**	**Pt-mtn**
Chemical formula	$C_{12}H_{23}Cl_2NOPtS$	$C_{14}H_{27}Cl_2NOPtS$	$C_{14}H_{27}Cl_2NOPtS$
Molecular weight ($g \cdot mol^{-1}$)	495.37	523.42	523.42
Crystal system, space group	*Monoclinic, $P2_1/c$*	*Monoclinic, $P2_1/c$*	Orthorhombic, *Pbca*
Temperature (K)	150	150	150
a, *b*, *c* (Å)	12.7546 (18), 32.285 (5), 15.611(2)	13.405 (2), 9.4994 (14), 14.267(2)	19.6534 (16), 8.5150 (7), 21.5493 (17)
β (°)	90.421 (3)	102.871 (3)	90
V ($Å^3$)	6428.16	1771.1	3606.2 (5)
Z	16	4	8
Radiation type	Mo Kα	Mo Kα	Mo Kα
μ (mm^{-1})	9.183	8.338	8.190
Crystal size (mm)	0.12 x 0.11 x 0.07	0.18 x 0.08 x 0.07	0.33 × 0.25 × 0.13
Tmin, Tmax	0.615, 0.745	0.561, 0.746	0.551, 0.746
No. of measured, independent and observed [$I > 2\sigma(I)$] reflections	121659, 13309, 10507	24304, 4378, 3547	84848, 5512, 5117
Rint	0.067	0.046	0.025
$(\sin \theta/\lambda)max$ ($Å^{-1}$)	0.628	0.666	0.715
$R[F^2 > 2\sigma(F^2)]$, $wR(F^2)$, S	0.038, 0.065, 1.11	0.026, 0.058, 1.02	0.020, 0.039, 1.23
No. of reflections	13309	4378	5512
No. of parameters	597	184	193
$\Delta\rho_{max}$, $\Delta\rho_{min}$ (e $Å^{-3}$)	1.22, -1.51	2.45, -1.04	1.22, −1.68

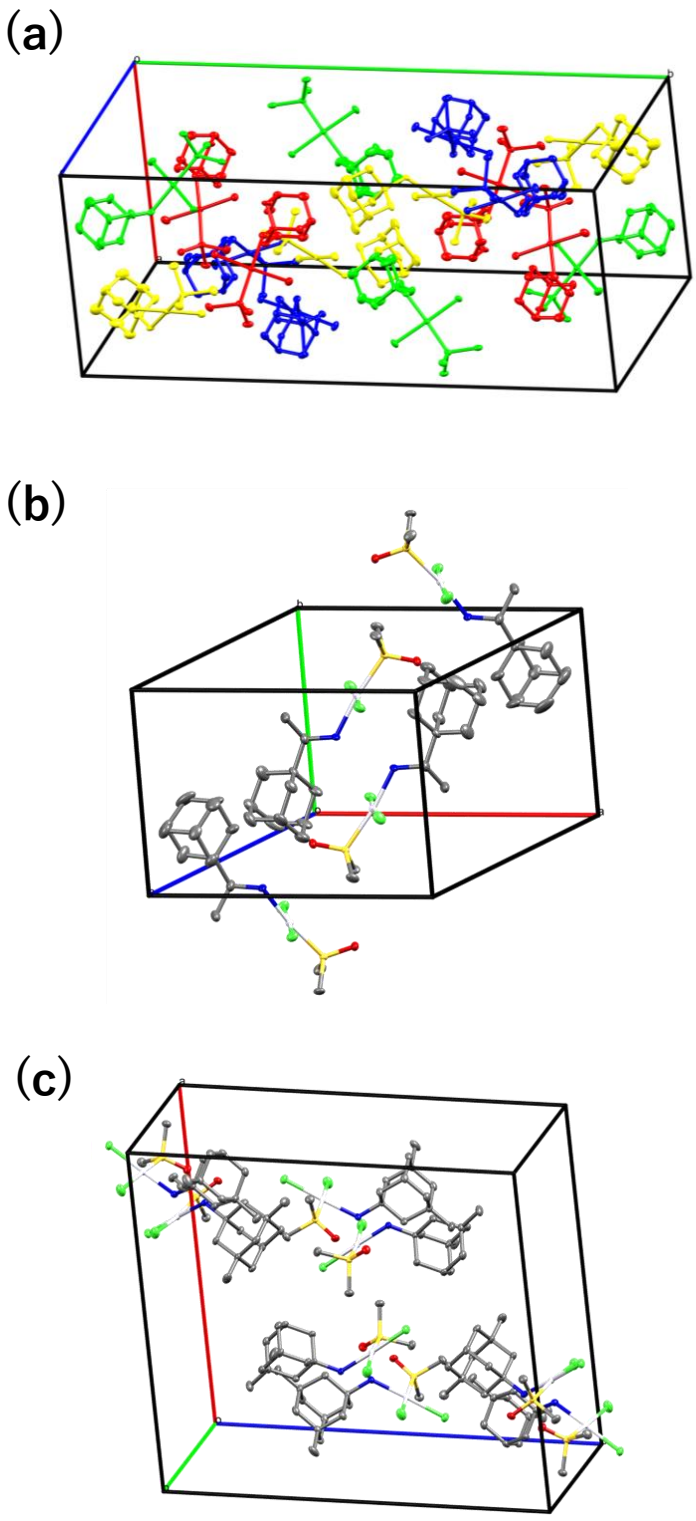

Figure S3. Crystal packing of (a) Pt-atd, (b) Pt-rtd and (c) Pt-mtn. *The four symmetrically independent Pt-atd molecules are color-coded: green - Pt1A, red - Pt1B, yellow - Pt1C, blue - Pt1D.

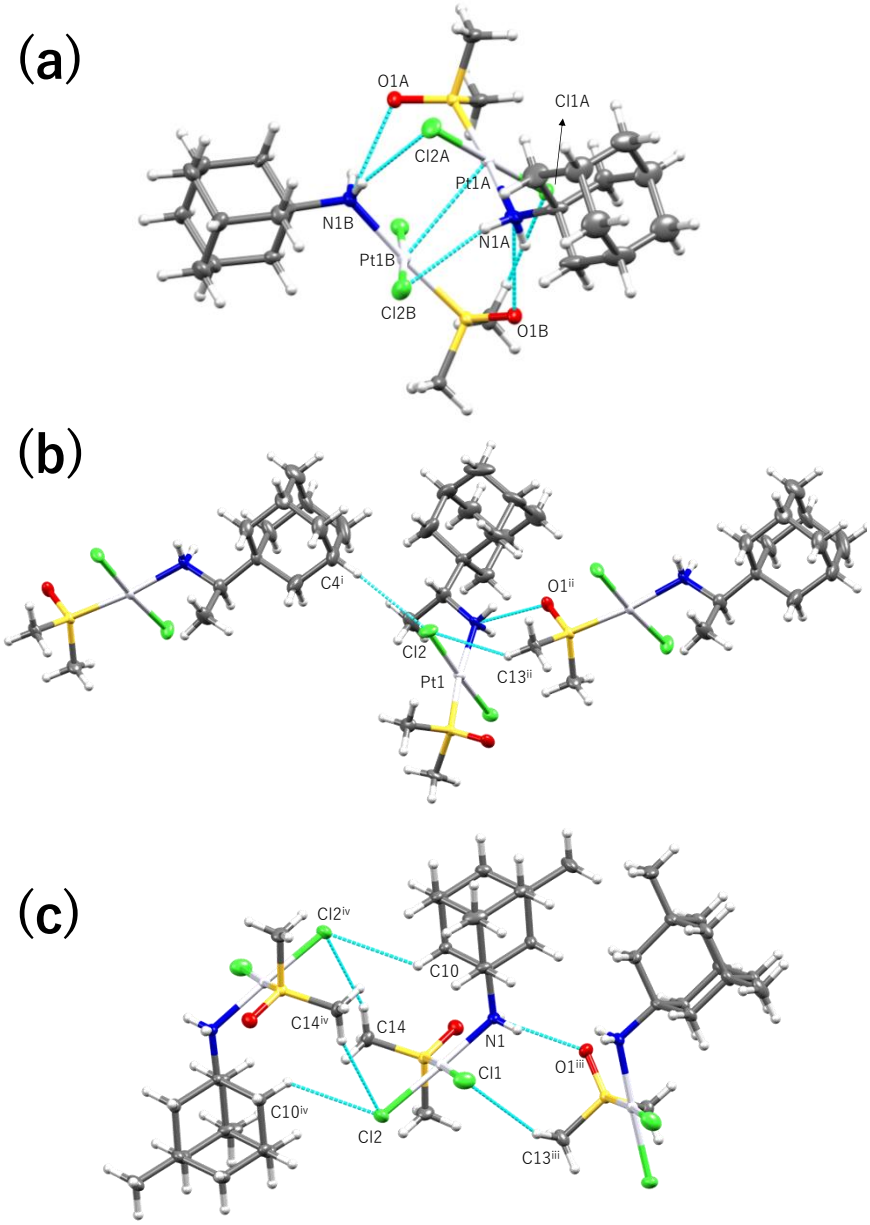

Figure S4. Intermolecular interactions in (a) Pt-atd, (b) Pt-rtd and (c) Pt-mtn. Symmetry codes: (i): -x, 1/2 + y, 1/2 – z; (ii): 1 – x, -1/2 + y, 1/2 – z; (iii): 3/2 – x, -1/2 + y, z; (iv): 1 – x, 1 – y, 1 – z.

Molecular modeling

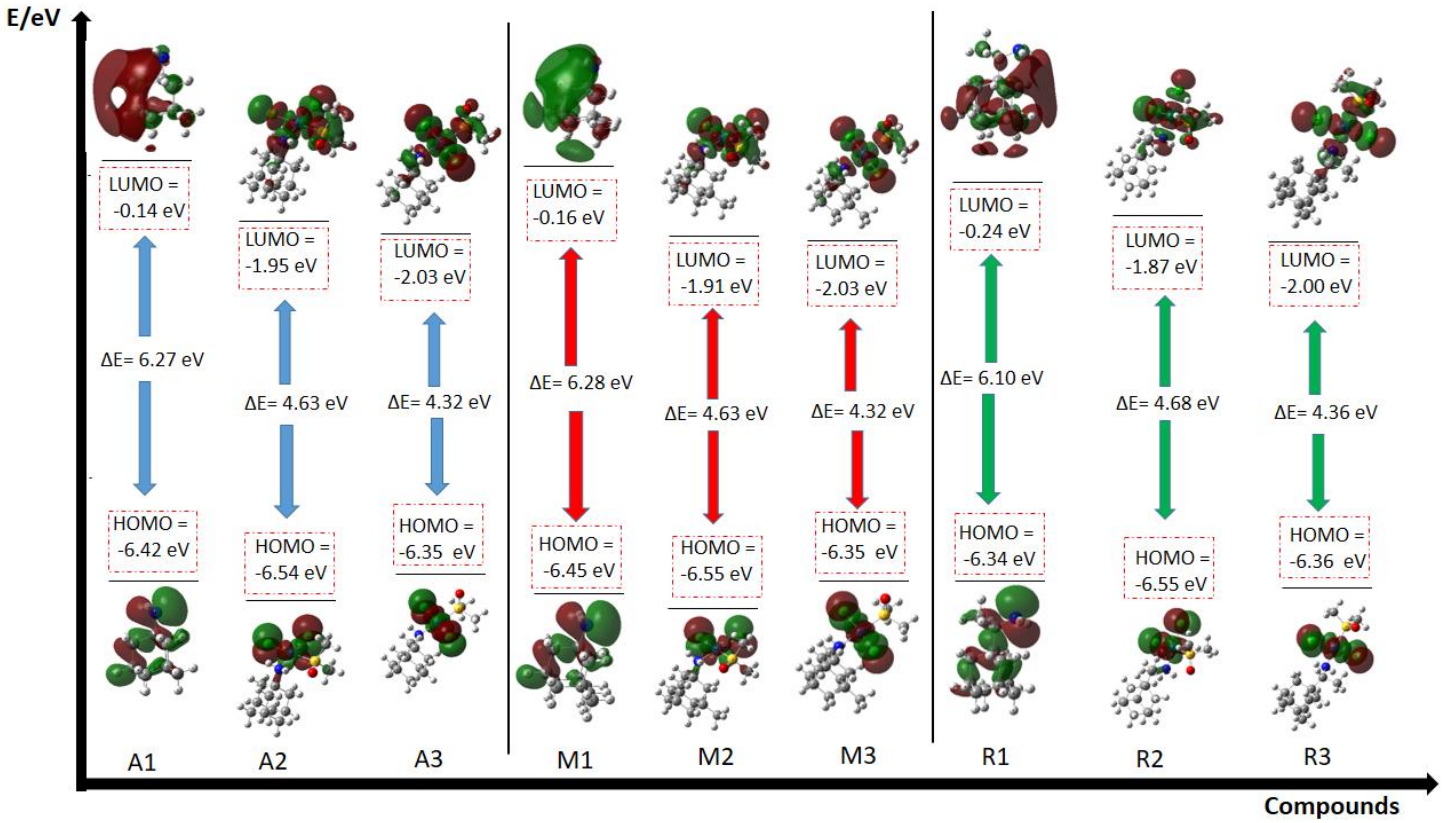

Figure S5. HOMO, LUMO and gap for: A1) atd, A2) *cis*-[$PtCl_2$(atd)(Me_2SO)], A3) *trans*-[$PtCl_2$(atd)(Me_2SO)], M1) mtn, M2) *cis*-[$PtCl_2$(mtn)(Me_2SO)], M3) *trans*-[$PtCl_2$(mtn)(Me_2SO)], R1) rtd, R2) *cis*-[$PtCl_2$(rtd)(Me_2SO)], R3) *trans*-[$PtCl_2$(rtd)(Me_2SO)]. Data obtained at the theory level B3LYP/6-31+G(d,p)/LANL2DZ. Me_2SO is dimethylsulfoxide.

Mass spectra

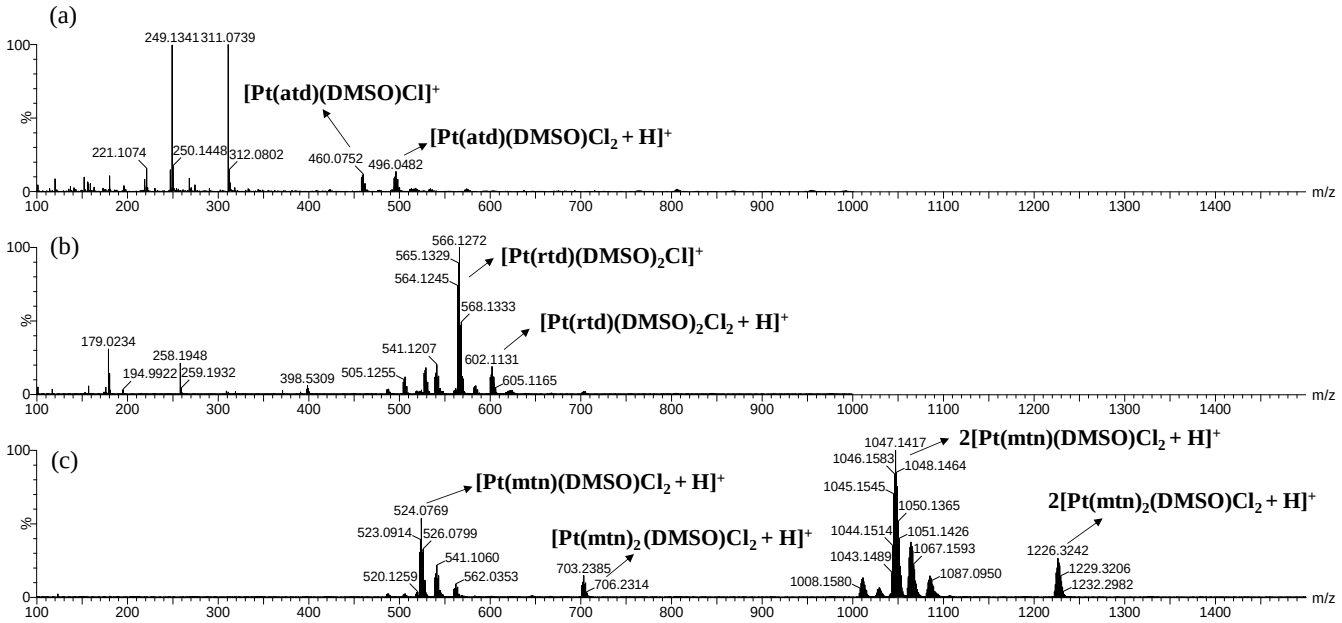

Figure S6. Mass spectra of (a) Pt-atd, (b) Pt-rtd and (c) Pt-mtn.

^{1}H NMR assignments and chemical shifts (ppm)

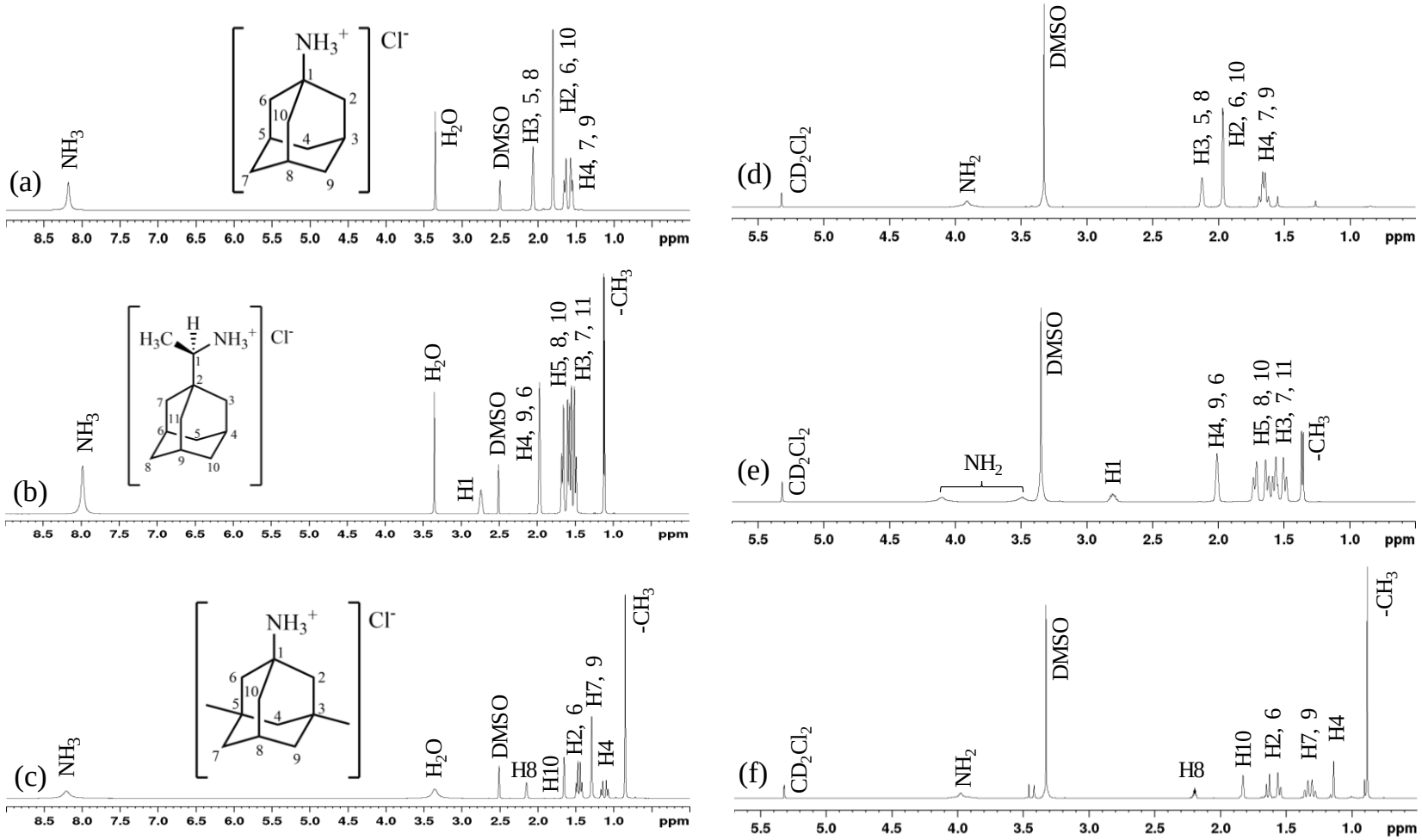

Figure S7. ^{1}H NMR spectra of (a) atdH, (b) rtdH and (c) mtnH in DMSO-d6 and of (d) Pt-atd, (e) Pt-rtd and (f) Pt-mtn in CD_2Cl_2

{^{15}N, ^{1}H} NMR 2D contour maps

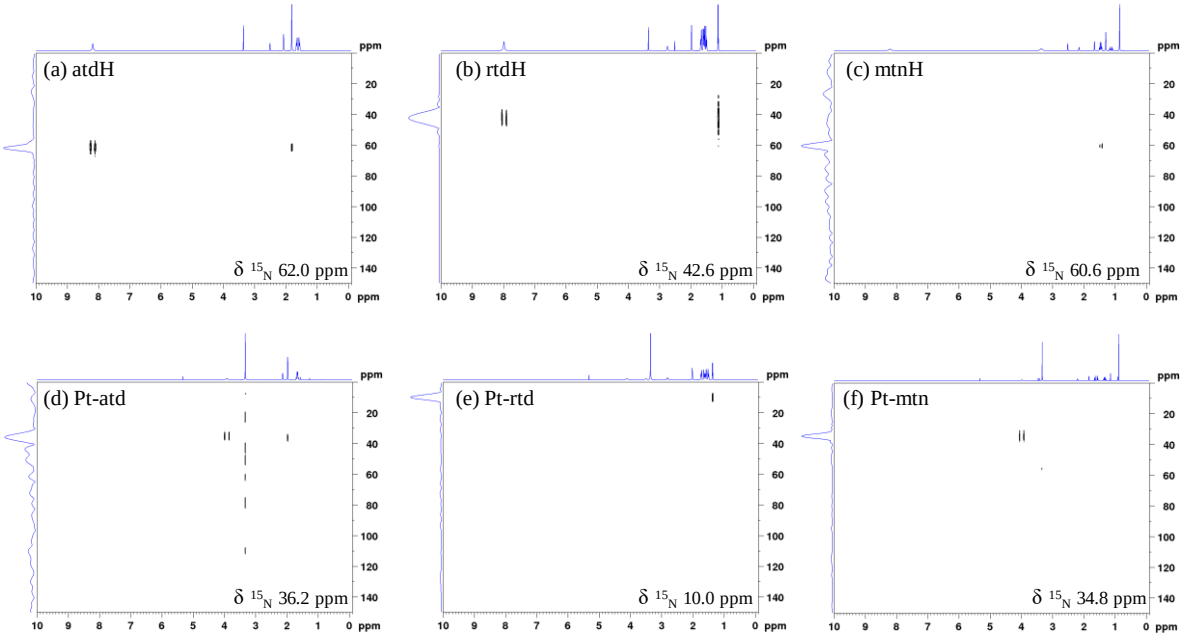

Figure S8. {^{15}N, ^{1}H} HMBC contour maps of (a) atdH, (b) rtdH, (c) mtnH in DMSO-d6 and of (d) Pt-atd, (e) Pt-rtd and (f) Pt-mtn in CD_2Cl_2.

^{1}H NMR kinetics studies

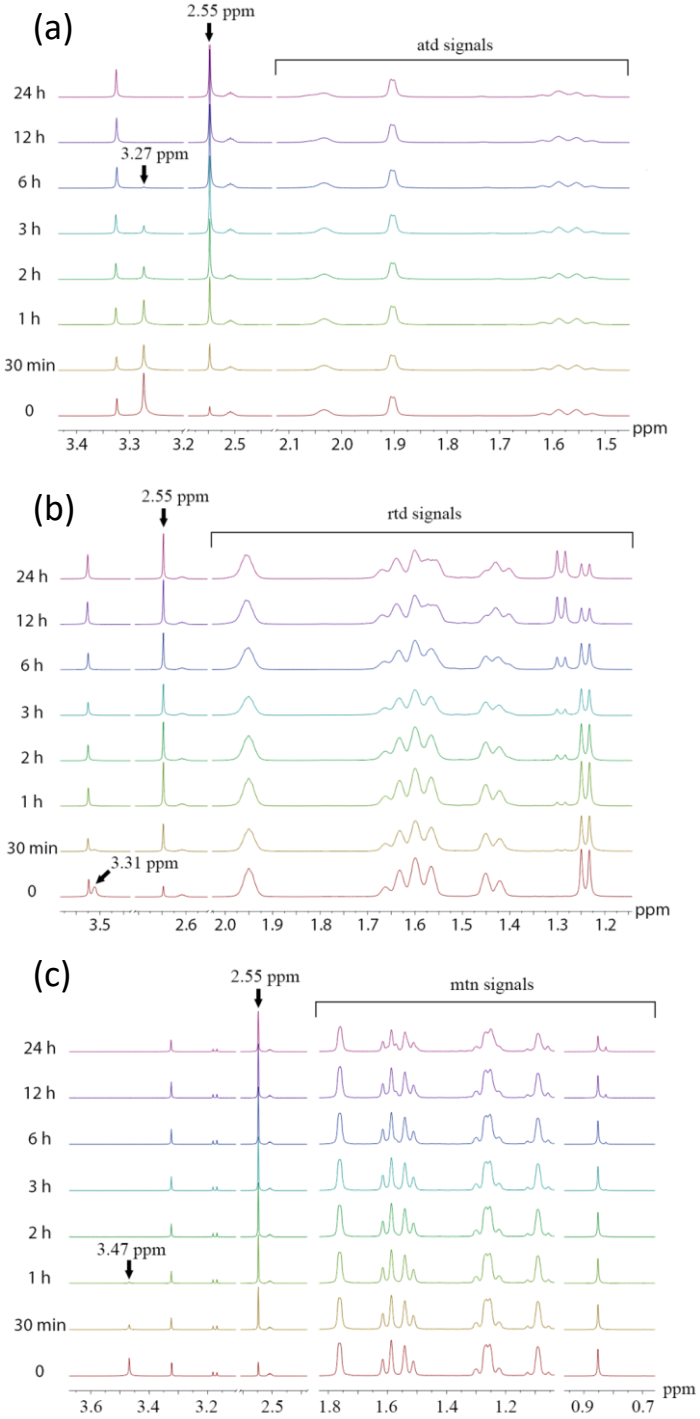

Figure S9: Kinetic studies of (a) Pt-atd, (b) Pt-rtd and (c) Pt-mtn for 24 hours, followed by ^{1}H NMR. Signals of coordinated DMSO (close to 3.3 ppm) and uncoordinated DMSO (2.55 ppm) are indicated by the arrows. For Pt-rtd and Pt-mtn the intensity of the signals between 1.00 and 1.80 ppm were increased for improved visualization.

Interaction with DNA

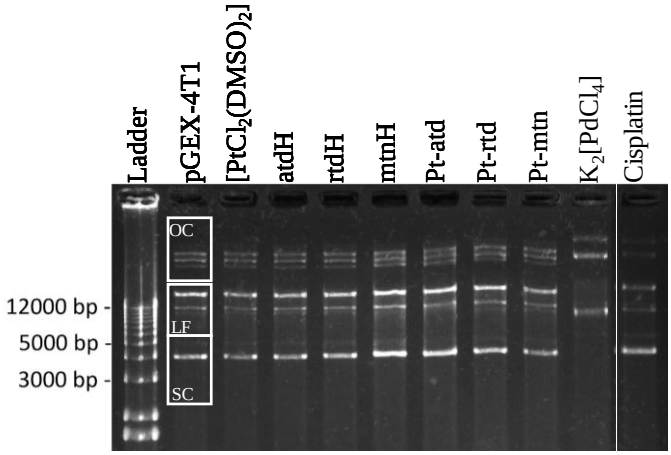

Figure S10: Agarose gel electrophoresis for the pGEX-4T1 plasmid DNA in the presence of the compounds at concentrations of 80 μmol·L^{-1}. OC = Open circular, LF = linear form and SC= supercoiled forms of the plasmid.

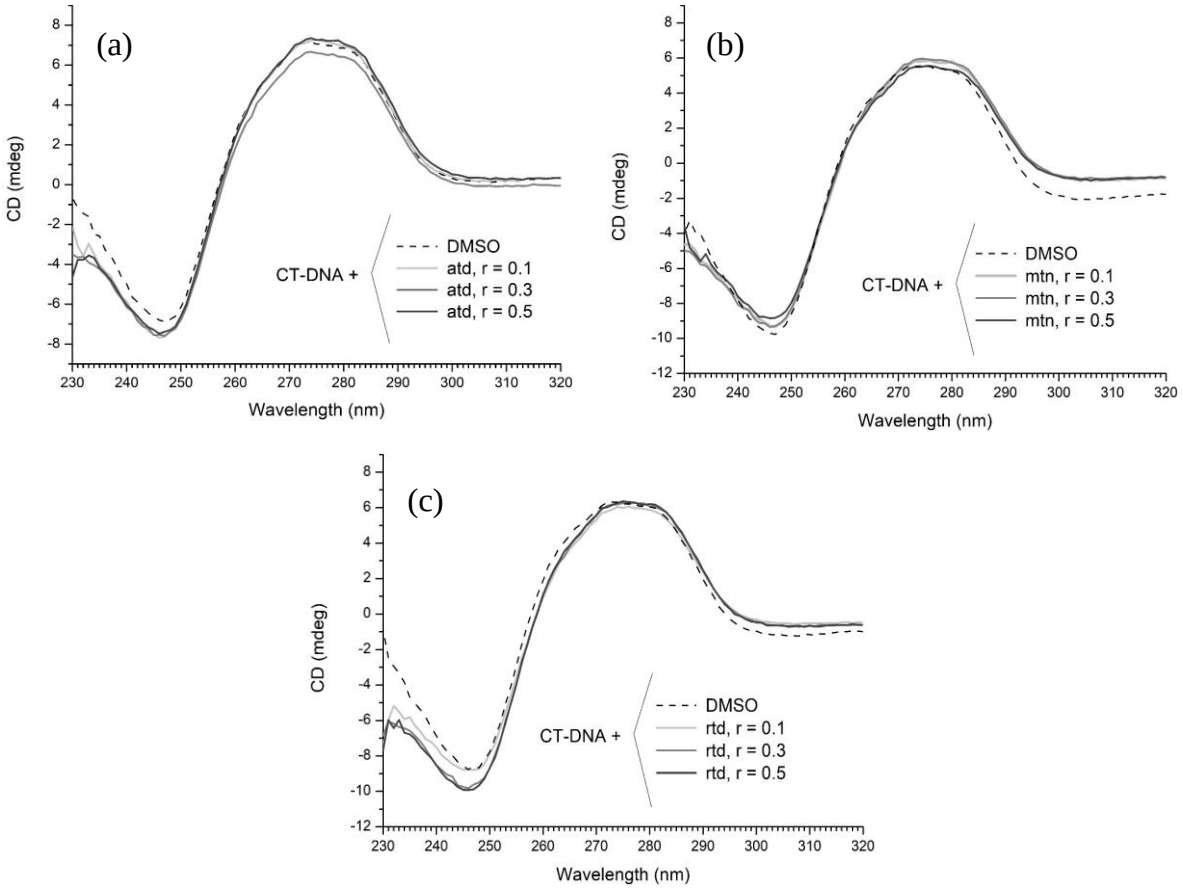

Figure S11. Circular dichroism spectra of CT-DNA (100 μM) in the absence and presence of (a) amantadine hydrochloride (b) rimantadine hydrochloride and (c) memantine hydrochloride at r = 0.1, 0.3 and 0.5.

Interaction with BSA

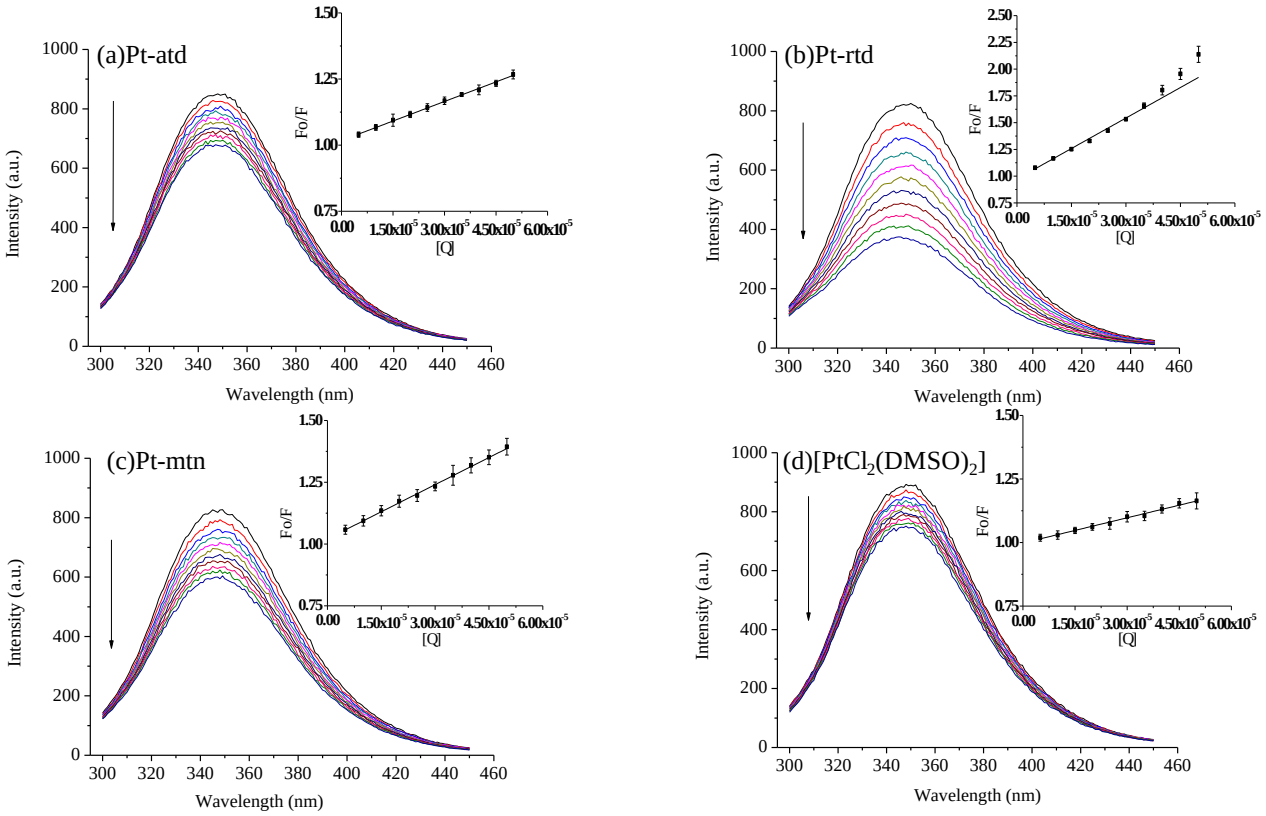

Figure S12: Fluorescence spectra of BSA in the absence and presence of the (a) Pt-atd, (b) Pt-rtd, (c) Pt-mtn and (d) $[PtCl_2(DMSO)_2]$ complexes. [BSA] = 2.4×10^{-6} µmol·L^{-1}. [Complexes] = 0.0, 5.0, 10.0, 15.0, 20.0, 25.0, 30.0, 35.0, 40.0, 45.0 and 50.0 µmol·L^{-1}.

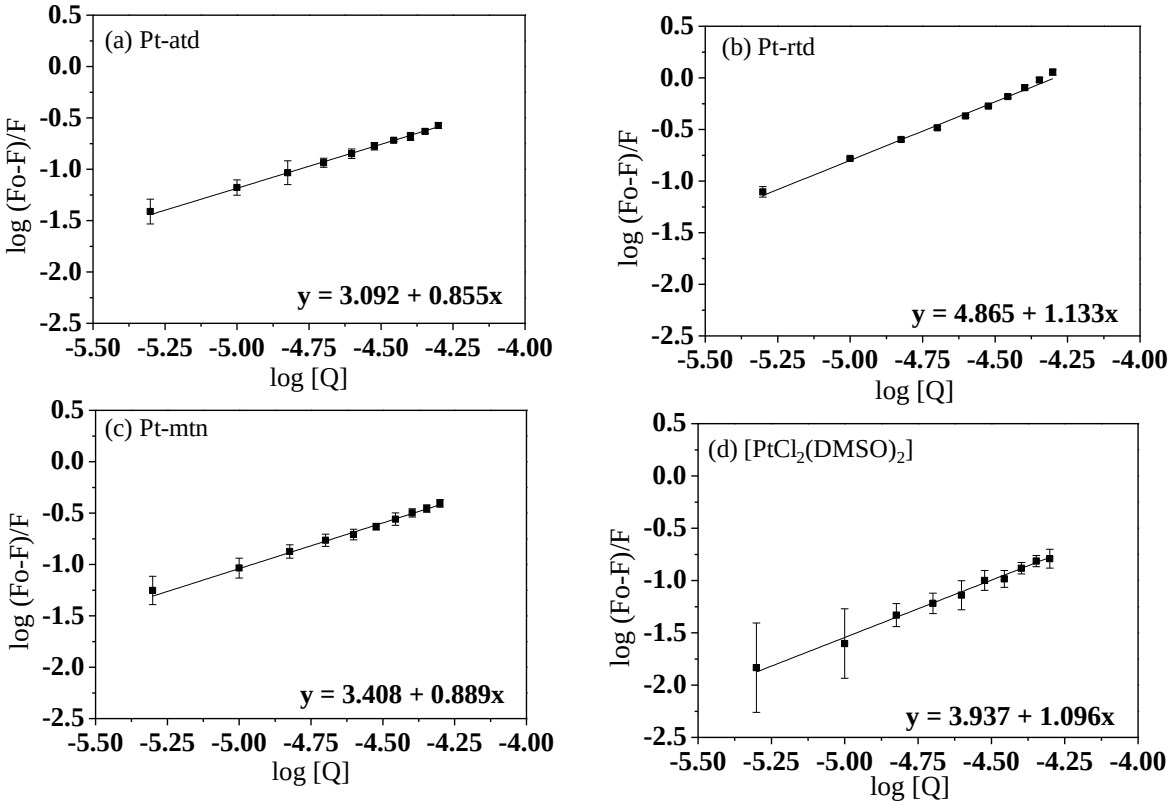

Figure S13. Plots for the interaction of (a) Pt-atd, (b) Pt-rtd, (c) Pt-mtn and (d) $[PtCl_2(DMSO)_2]$ complexes with fluorescence maxima of BSA at 347 nm.

References

1 J. C. Garcia, J. F. Justo, W. V. M. Machado and L. V. C. Assali, *J. Phys. Chem. A*, 2010, **114**, 11977–11983.

2 S. Podunavac-Kuzmanovic, D. Cvetkovic and L. Vojinovic, *Acta Period. Technol.*, 2004, **35**, 239–246.

3 D. Jeremic, M. Djordjevic, S. Miletic, L. Andjelkovic, D. Sladic and I. Brceski, *J. Serbian Chem. Soc.*, 2018, **83**, 699–705.

4 P. Van Thong, D. T. Thom, N. Thi and T. Chi, 2018, **56**, 146–151.

5 V. Y. Kukushkin, V. K. Belsky, V. E. Konovalov, G. A. Kirakosyan, L. V. Konovalov, A. I. Moiseev and V. M. Tkacbuk, *Inorganica Chim. Acta*, 1991, **185**, 143–154.